



## CARBON BASED SMART SYSTEM FOR WIRELESS APPLICATION



Start Date : 01/09/12  
Project n°318352

Duration : 36 months

Topic addressed : Very advanced nanoelectronic components: design, engineering, technology and manufacturability

### WORK PACKAGE 2 : Design and simulation activities

#### DELIVERABLE D2.5

#### Report on design of graphene devices

Due date : T0+12

Submission date : T0+13

Lead contractor for this deliverable : IMT

Dissemination level : PU – Public

	<b>D2.5 : Report on the design of graphene devices</b>	2/30
---	--	------

## WORK PACKAGE 2 : Design and simulation activities

### PARTNERS ORGANISATION APPROVAL

	Name	Function	Date	Signature
Prepared by:	Mircea Dragoman	Senior researcher 1	24/09/2012	
Prepared by:	Stephane XAVIER	R&D Engineer	27/09/2013	
Approved by:	Afshin Ziaei	Research Program Manager	30/09/13	

### DISTRIBUTION LIST

QUANTITY	ORGANIZATION		NAMES
1 ex	Thales Research and Technology	TRT	Afshin ZIAEI
1 ex	Chalmers University of Technology	CHALMERS	Johan LIU
1 ex	Foundation for Research & Technology - Hellas	FORTH	George KONSTANDINIS
1 ex	Laboratoire d'Architecture et d'Analyse des Systèmes	CNRS-LAAS	George DELIGEORGIS
1 ex	Université Pierre et Marie Curie	UPMC	Charlotte TRIPON-CANSELIET
1 ex	National Research and Development Institute for Microtechnologies	IMT	Mircea DRAGOMAN
1 ex	Graphene Industries	GI	Peter BLAKE
1 ex	Thales Systèmes Aéroportés	TSA	Yves MANCUSO
1 ex	SHT Smart High-Tech AB	SHT	Yifeng FU
1 ex	Universita politecnica delle Marche	UNIVPM	Luca PIERANTONI
1 ex	Linköping University	LiU	Rositsa YAKIMOVA
1 ex	Fundacio Privada Institute Catala de Nanotecnologia	ICN	Clivia SOTOMAYOR
1 ex	Tyndall-UCC	Tyndall	Mircea MODREANU

	<b>D2.5 : Report on the design of graphene devices</b>	3/30
--	--	------

## CHANGE RECORD SHEET

REVISION LETTER	DATE	PAGE NUMBER	DESCRIPTION
Template	07/2013		
V1	25/09/2013	30	IMT contribution

## CONTENTS

1	INTRODUCTION .....	6
2	GRAPHENE ANTENNA .....	7
3	LOW NOISE GRAPHENE AMPLIFIER .....	13
4	THE DETECTOR .....	20
5	THE GRAPHENE MIXER .....	25
6	CONCLUSION .....	28

## **ABBREVIATION / DEFINITION**

**CPW**      Coplanar waveguide

### 1 INTRODUCTION

Graphene is a graphite monolayer with a thickness of only 0.34 nm, formed of carbon atoms in a hybridization state of  $sp^2$ , so that each atom is covalently bonded to three others. Graphene is also a two dimensional (2D) crystal and a natural 2D gas of charged particles. The ballistic transport of carriers in graphene takes place at room temperature over a distance of 0.4  $\mu\text{m}$  and reaches an intrinsic mobility of 44 000  $\text{cm}^2\text{V}^{-1}\text{s}^{-1}$  [1]. However, when graphene is deposited with a hexagonal boron nitride substrate [2] matching the graphene lattice, mobilities higher than 100 000  $\text{cm}^2/\text{s}$  and mean-free carrier paths of 1  $\mu\text{m}$  are measured at room temperature. Due to these electrical properties, that are superior by orders of magnitude to those of semiconductors and semiconductor heterostructures, graphene is seen as a promising material for ultrafast nanoelectronic devices such as transistors with cutoff frequencies beyond 100 GHz, and optical devices, for example photodetectors; it could also be used as a transparent electrode for photovoltaic applications [3], [4]. The main challenge is to transfer these physical graphene properties into RF devices and circuits.

The electromagnetic properties of graphene in RF, microwave, millimeter waves are not well known and studied. Coplanar metallic lines deposited on graphene transferred on  $\text{Si}/\text{SiO}_2$  were studied and it was demonstrating that graphene is working as a DC voltage tunable matching device [5], and that the contact resistance – a serious issue in graphene is shorted beyond few GHz, the graphene devices behaving contactless during the measurements up to 110 GHz [6]. The microwaves based on graphene are scarce except graphene transistors extensively studied by many groups in the world (see [3] for a comprehensive review).

This deliverable is dealing with the graphene devices design in NANORF project. In fact, in NANORF the high frequency devices are forming a receiver. Therefore, we will report on graphene antenna, graphene amplifier and a graphene rectifier. Adding a graphene mixer we will have a heterodyne receiver the best receiver knows in terms of low noise performances and sensitivity. However, the existing graphene mixers are not able to provide a conversion loss enough low to be used in a heterodyne receiver. Therefore, we will use a Schottky diode to perform this task. We note that many of the above devices were either **not** experimented not known and up to now so this WP is very challenging. The ultimate goal is to have a microwave receiver based on graphene.

In Nano-RF project the second demonstrator is represented below (Figure 1):

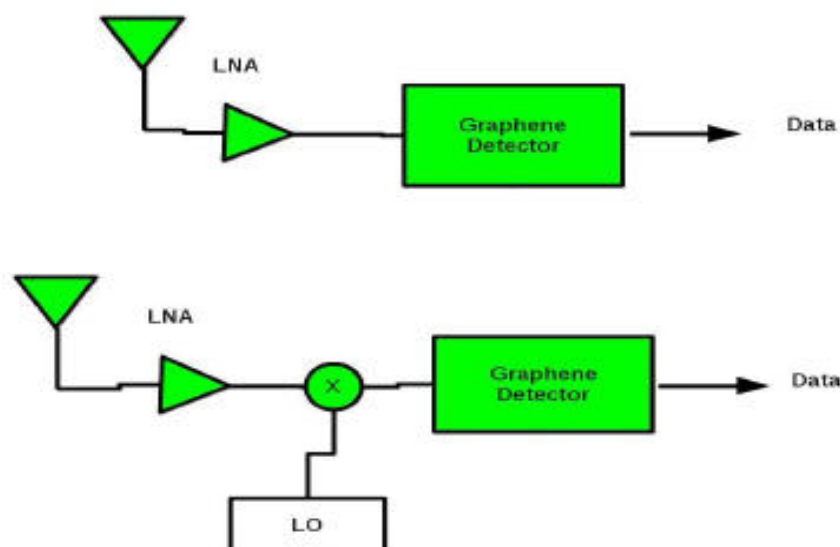


Figure 1 : Second demonstrator in Nano-RF project

The first receiver is a direct microwave receiver while the second is a microwave heterodyne receiver. Since the second solution is very risky, Nano-RF has proposed two solutions hoping to implement at least one of them, but we hope that both solutions will be finally successfully implemented.

We note that green colour is used to indicate the devices to be fabricated in Nano-RF.

## 2 GRAPHENE ANTENNA

Since nowadays the graphene monolayer is grown by CVD techniques on SiO<sub>2</sub>/Si wafers with 4 inch diameters we can imagine that an entire receiver could be fabricated on a such big wafer.

The basic configuration of the graphene antenna is depicted in Figure 2. This is a coplanar waveguide (CPW) patch antenna. The patch is rectangular graphene monolayer sheet (blue) excited by a CPW. The ground of CPW is surrounding the patch antenna allowing radiations via the slots created by the graphene patch and the graphene patch. There are previous reports about such antenna with a metal resonator (see [7] and the reference herein]. However, as we will see further the graphene resonator provide to antenna new functionalities. The initial data for simulation with HFSS were :

- $f_0 = 10 \text{ GHz}$ ,
- $\lambda_g = 1.8 \text{ cm}$ ,
- $W \cong \lambda_g / 2 = 0.9 \text{ cm}$ ,
- $L \cong 0.1\lambda = 0.18 \text{ cm}$
- $S = 450 \mu\text{m}$ .

The CPW ground electrodes width are considered as  $6S = 2.7 \text{ mm}$  and  $A = 100 \mu\text{m}$ ,  $B = 50 \mu\text{m}$ .

The graphene electrical permittivity is 3.3 (see WP3.2 deliverable where we report the measurement of this important parameter).

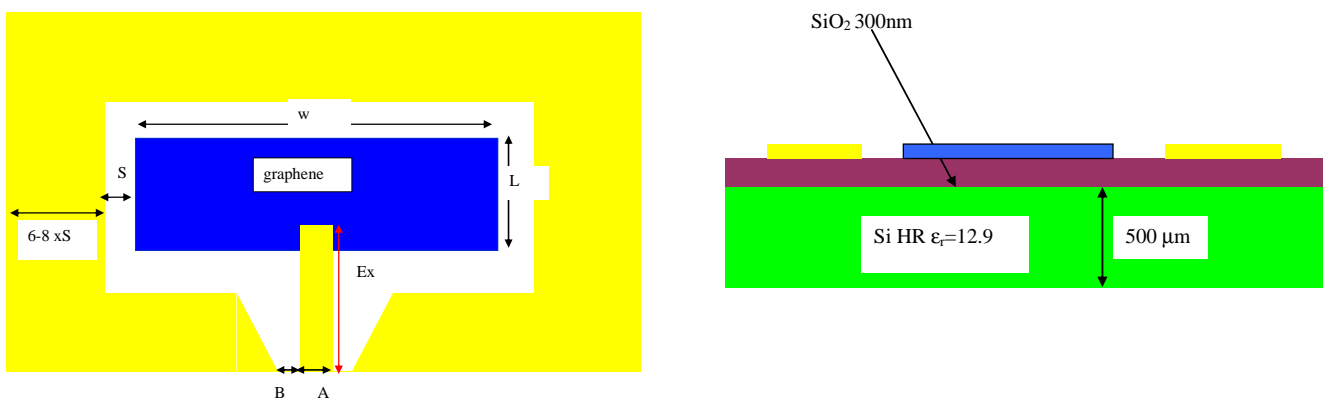


**Figure 2 : The configuration of graphene antenna**

The real part of the intraband term of conductivity is dominating over an ultrawideband range of frequencies starting from DC and ending at 2-3 THz. In the same range of frequencies, the imaginary part is very small ([8],[9]).

The intraband conductivity is given by:

$$\sigma(\omega) = -ie^2 k_B T / \pi \hbar^2 (\omega - i2\Gamma) [(\mu / k_B T) + 2 \ln(\exp(-\mu / k_B T) + 1)] \quad (1)$$

where  $\mu$  is chemical potential  $\mu \equiv e\alpha V_b$  with  $V_b$  as bias voltage and  $\alpha$  - a constant depending on the geometry of the device,  $T$  is the temperature and  $\Gamma$  is a scattering rate independent of energy,  $\Gamma = 1/\tau$ , with  $\tau = 1ps$ .

The surface impedance is given by :

$$Z_s(V_b) = 1/\sigma(\omega) = R_s(V_b) + jX_s(V_b) \quad (2)$$

Where  $R_s$  takes values in the range  $50\Omega$ - $2k\Omega$  depending on applied voltage, while  $X_s = 0.2 - 3\Omega$  without any influence on further results. From (2) we can see that  $Z_s$  is depending on bias voltage which can tune it.

The graphene surface resistance  $R_s(V_b)$  can be tuned by a DC voltage applied on CPW  $500\Omega$ -  $1k\Omega$  [8] ,[9] ,[10] the highest value  $1$ - $2 k\Omega$  is at  $0V$ . The graphene surface resistance value is nearly independent of frequency up to  $2 THz$  [11] when interband conductivity becomes important. In Figure 3 we can see the effects described above. The antenna S11 reflection coefficient is tuned via applied DC voltage. In the figure it is depicted the surface resistance and the DC voltage necessary to be obtain the corresponding  $R_s$ .

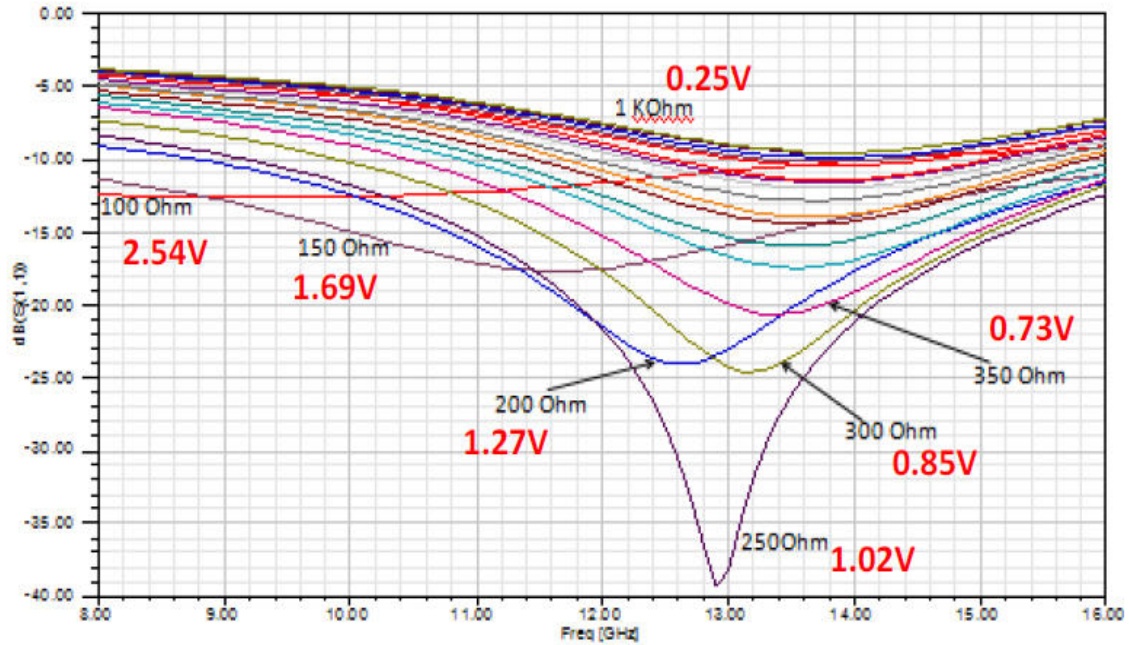


**Figure 3 : The simulated S11 at various  $R_s$**

While at high surface resistances the VSWR is high but still good for antennas (VSWR=3) when antenna is biased the VSWR is reduced nearly to 1 attaining for 10 GHz 1.5. The best result is obtained at 13 GHz where the VSWR is only 1.02.  $R_s(V_b)$ .

So, we can tune the antenna in the range 10-15 GHz to get the maximum performances.



This new effect not previously used in any antenna and is entirely due to graphene where the surface resistance is dependent on the applied voltage.

The first simulation we have done having  $R_S = 250 \Omega$ . The radiation pattern is depicted in Figure 4. However, the S11 was unsatisfactory and the radiation efficiency was 12 % which is quite low.

We have increased  $R_S = 500 \Omega$  and we get a VSWR of 3.2 which could be accepted but the radiation efficiency has increased at 13 % .Increasing the surface resistance at  $700 \Omega$  we get a radiation efficiency of 95 % at 13 GHz, the radiation pattern is similar with Fig.3 and will be not reproduced here.

We note that this is the surface resistance of graphene CVD grown graphene to be used for the graphene antenna fabrication. Since we can change the resonance of the antenna changing the bias, we choose the frequency of 13 GHz and the  $R_S = 250 \Omega$  and we get the S11 depicted in Figure 5 a VSWR of 1.02 at 13 GHz and the efficiency is given by :

$$(\iint |E_t|^2 / Z_S) / \text{input power} = 0.73$$

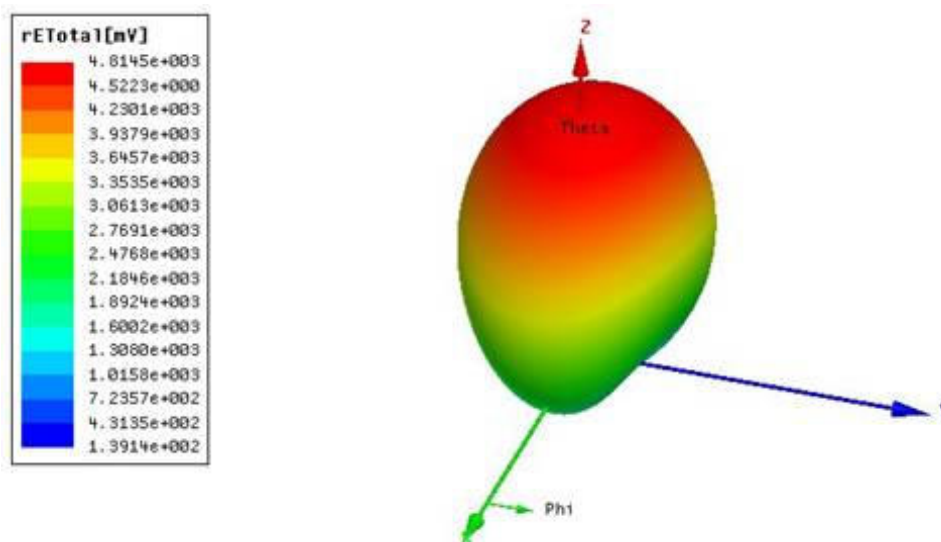


Figure 4 : The radiation pattern when  $R_S = 250 \Omega$

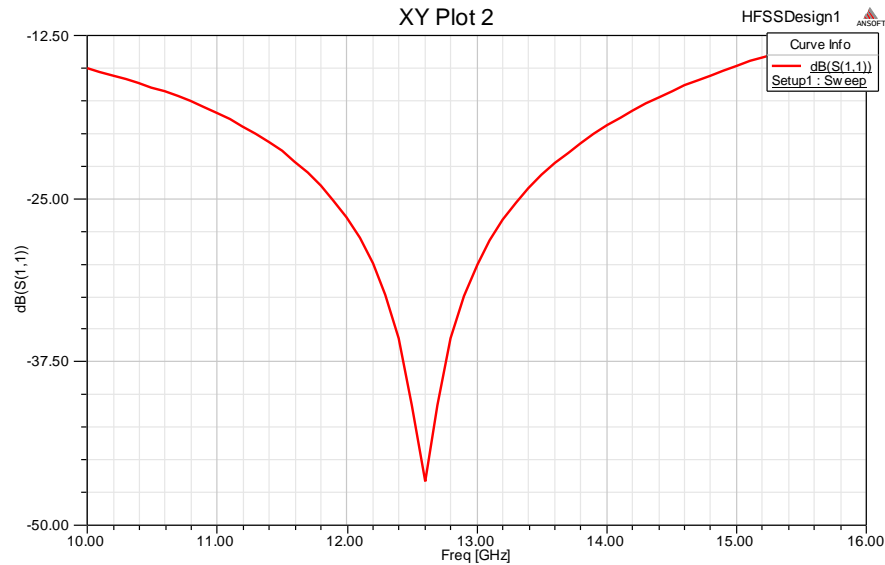


Figure 5 : S11 at 13 GHz and  $R_s = 250 \Omega$

An optimized graphene antenna is represented in Figure 6 where  $L_s = 8950 \mu\text{m}$ .

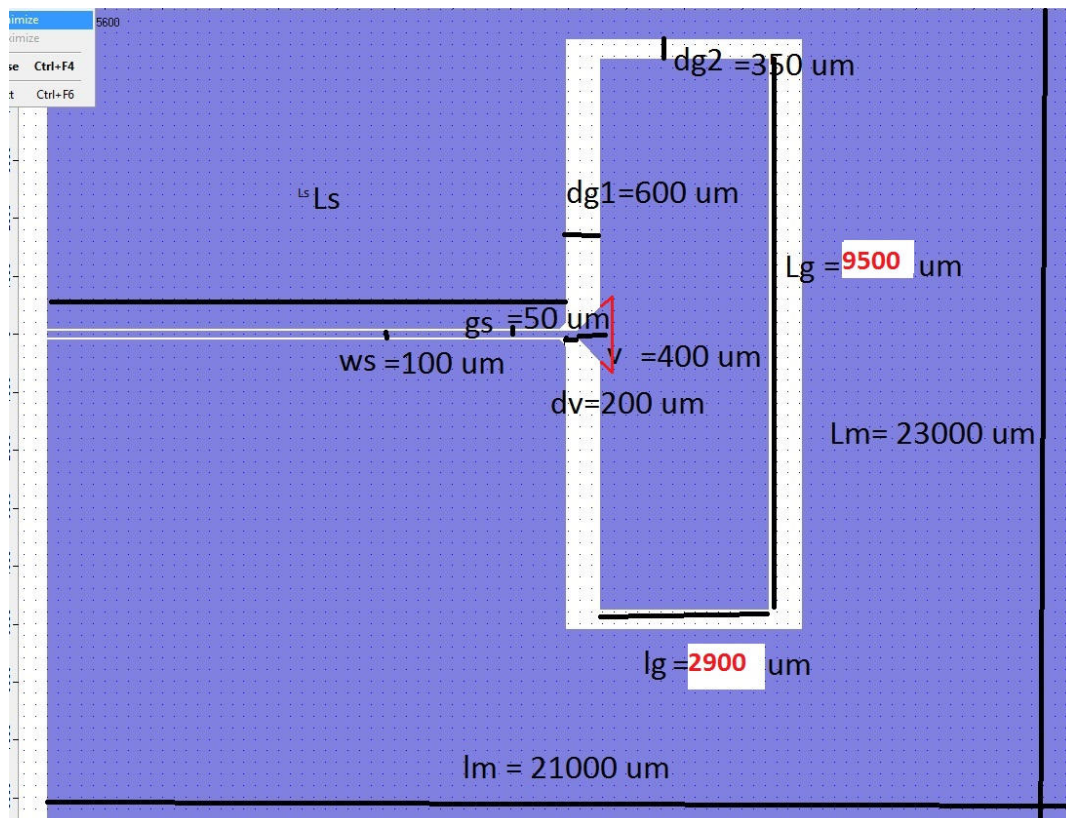


Figure 6 : The optimized graphene antenna.

The S11 parameter is displayed below in Figure 7. The VSWR at resonance is 1.4 while the other antenna parameters are represented in Figure 8.

We see from Figure 8 that we get a pretty good efficiency of 79 %

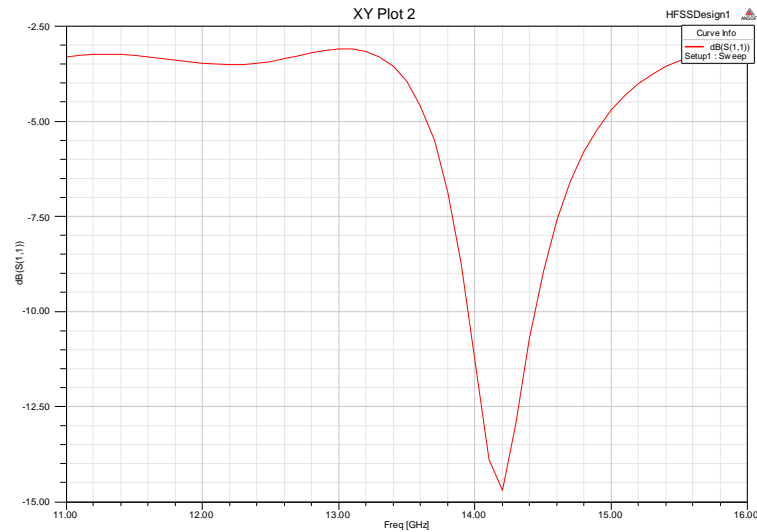


Figure 7 : S11 for the optimized antenna.

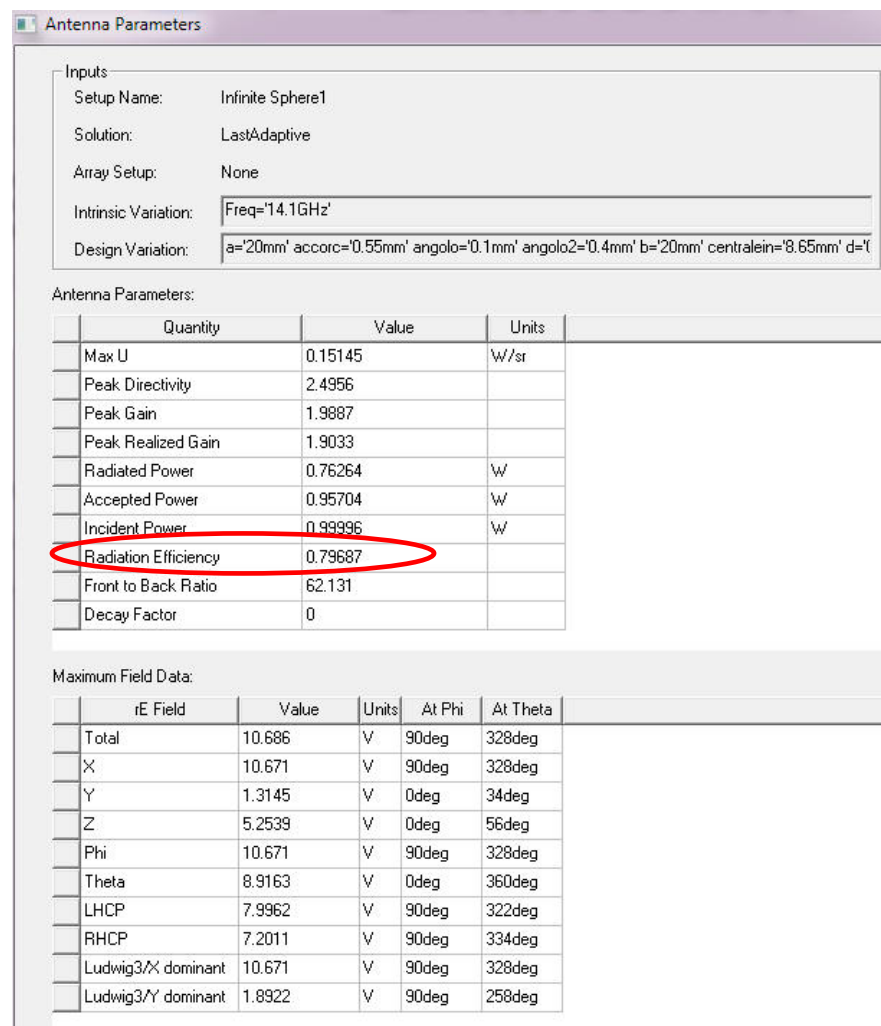


Figure 8 : The graphene antenna optimized performances.

We have used also the CST to simulate the antenna and even if the results using two different simulators based on two different ways to solve Maxwell simulation (HFSS –solving Maxwell’s equations in frequency domain and the CST in domain) are different CST simulator has given us supplementary information summarized in Table 1.

8÷16 GHz	<i>Even mode</i>	<i>Odd mode</i>
<i>Z<sub>port</sub></i>	~ 50 $\Omega$	~ 119 $\Omega$
<i>f<sub>res</sub></i>	~ 10.4 GHz	~ 10.7 GHz
<i>f<sub>best matching</sub></i>	~ 11 GHz	~ 9.5 GHz
<i><math>\eta</math></i>	~ 2.4%	~ 66%
<i>BW<sub>-10 dB</sub></i>	~ 4 GHz	~ 4 GHz

Table 1 : CST results

The CST simulation of the graphene antenna shows similar results with HFSS only if the excitation of the antenna is only in odd mode. When the graphene antenna is fabricated and we will obtain not satisfactory results, we will add a coupler at antenna input to be excited only in the odd mode. The CST simulations have used the same dimensions as the above graphene antennas. The S11 reflection coefficient for the odd mode is good and it is depicted in Figure 9.

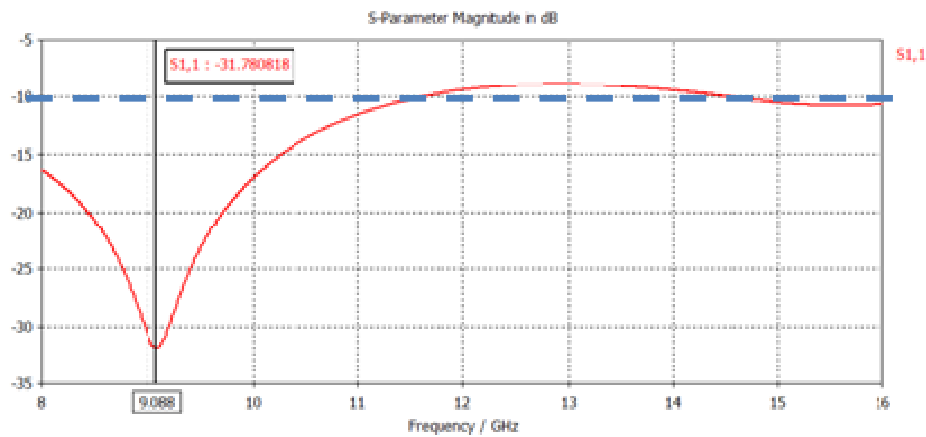


Figure 9 : S11 of the odd mode excitation.

The odd excitation radiation pattern is depicted in Figure 11 where the graphene antenna coordinates are depicted in Figure 10.

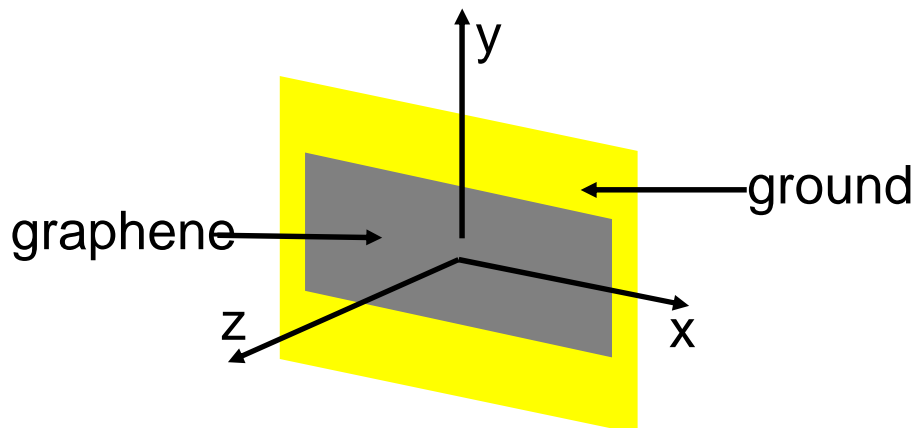


Figure 10 : Graphene coordination system in CST simulation.

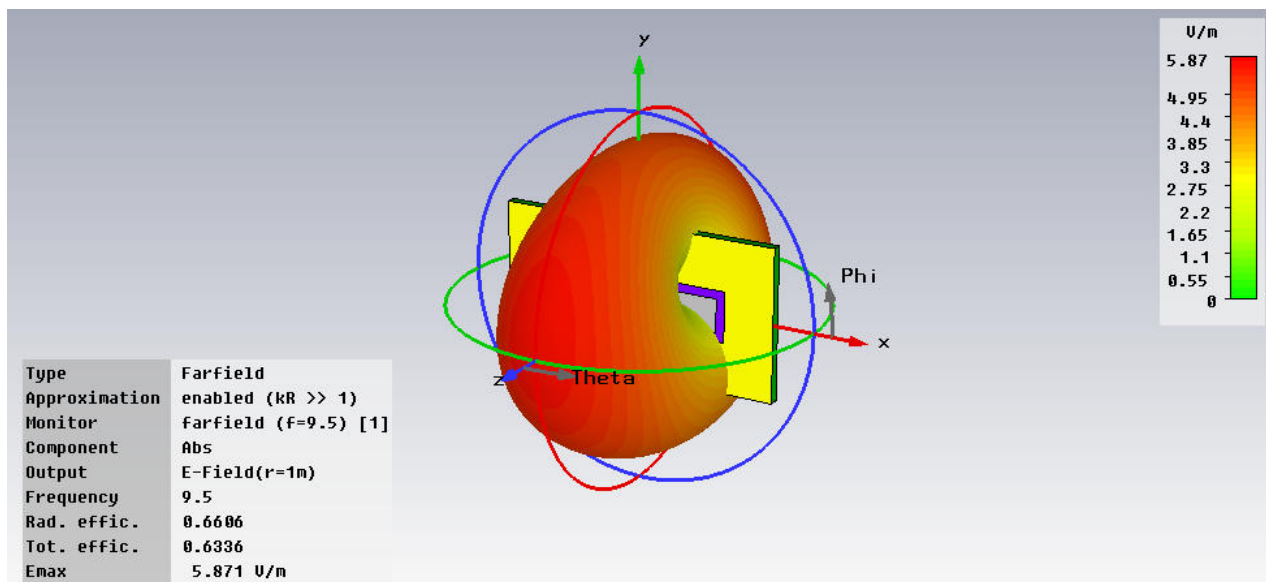


Figure 11 : The graphene antenna radiation pattern at 9.5 GHz using CST.

We can see from above figure that the radiation efficiency is excellent.

### 3 LOW NOISE GRAPHENE AMPLIFIER

The main issue of a low noise amplifier is to design a proper graphene FET. We have designed first (a) quasi ballistic graphene FET (b) and (c) two distinct methods for the design of the ballistic graphene FET.

The graphene FET uses graphene (monolayer or bilayer) as a channel which is modulated by a gate or two gates. The configuration of the graphene FET can have various versions. If the substrate is a doped Si this is acting as a metal-like and as a back gate (BG) able to modulate the carrier density in graphene channels. If the Si substrate is of high-resistivity or is SiC then there is need of a top-gate (TG) to modulate the carrier density in graphene channel (TG). However, a combination TG and BG is possible for some graphene transistors. The oxide used for isolation of the metal gates is usually

SiO<sub>2</sub>, but especially for the top oxides Al<sub>2</sub>O<sub>3</sub> or HfO<sub>2</sub> can be used. For the top gates the thickness of oxides is ranging between few nm and 100 nm. Although the graphene FETs have reached cutoff frequencies of 300 GHz there is a lot of room in the improvements of graphene FET performances.

The enhanced performances are expected to come from TG configurations, since the doped substrates are lossy in microwaves and millimeterwaves. As we will see the graphene contact resistance is main obstacle against outstanding performances of graphene FETs.

Considering a graphene FET in TG configuration, so having an insulating substrate as it is depicted in Figure 12.

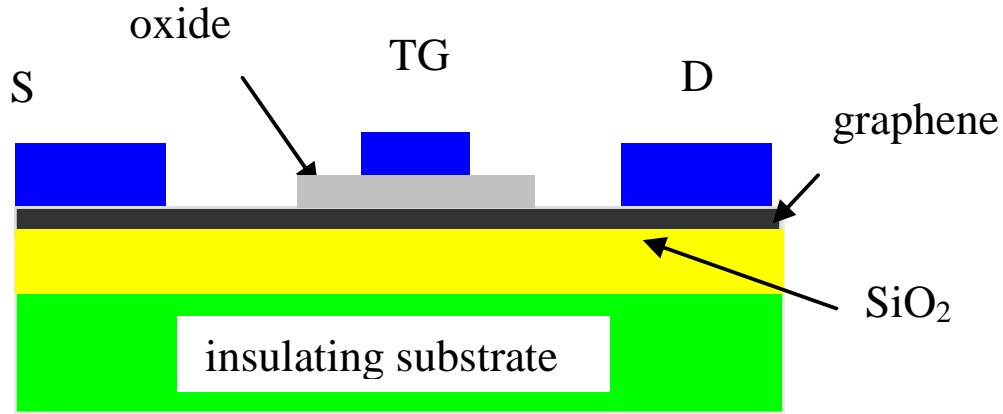


**Figure 12 : The configuration of the graphene transistor with top gate.**

We will denote the gate length as  $L$  and its width is  $W$  and the potential surface as  $\varphi(x)$ , where  $x$  is the position in the channel. If we consider the quantum capacitance limit, case in which the gate capacitance  $C_{ox}$  is much greater than the quantum capacitance  $C_Q$ . In this case the channel voltage form can be simplified and written as [13]:

$$V_{CH} = (x/L)V_{DS} \quad (3)$$

In this case, the drain is given by [Y4]:

$$I_D(V_D, V_G) = e(W/L)\mu^*V_{DS}[n_0 + \gamma(V_{GS}^2 + V_{DS}^2/3 - V_{DS}V_{GS})] \quad (4)$$

where  $n_0$  is the number of impurities considered to be  $10^{11}\text{cm}^{-2}$ ,  $\mu^* = \mu[1 + (\mu V_{DS}/v_{sat}L)]$

where  $\mu$  is the mobility of the graphene FET and  $\alpha$  is constant  $\gamma = e^2/\pi\hbar^2v_F^2$ . The saturation velocity is  $v_{sat} = v_F/2$ , where  $v_F$  is the Fermi velocity.

In the case when the mobility is not known, we can extract it from [Y5]:

$$\mu = \frac{1}{en} \frac{\partial I_D / W}{\partial V_D / L} \quad (5)$$

where  $n = \epsilon_0\epsilon_d V_g / te \cong \alpha V_g$ , and  $\epsilon_0$  and  $\epsilon_d$  are the dielectric permittivity of air and of the top dielectric with thickness  $t$ .

Considering that  $L=W=1\mu\text{m}$ , and that  $\mu = 3000\text{ cm}^2/\text{Vs}$ , the drain-voltage characteristic  $I_D - V_D$  for  $V_G = 0.5\text{ V}$ ,  $0.8\text{ V}$ ,  $0.9\text{ V}$ ,  $1\text{ V}$  is depicted in Figure 13.

We can see various curve shapes. At  $V_G=0.5\text{ V}$  it is evident the cubic dependence between the drain current and the drain voltage. The  $I_D - V_D$  is divided into three regions : (I) sublinear (II) saturation for which  $V_{DS} = V_{GS}$  corresponding to Dirac point and (III) superlinear. Then, as soon as the gate voltage is increasing, we will retrieve in the  $I_D - V_D$  dependence only the first two regions. The interesting case of  $I_D - V_D$  for  $V_G=0.5\text{V}$  is depicted separately in Fig.10

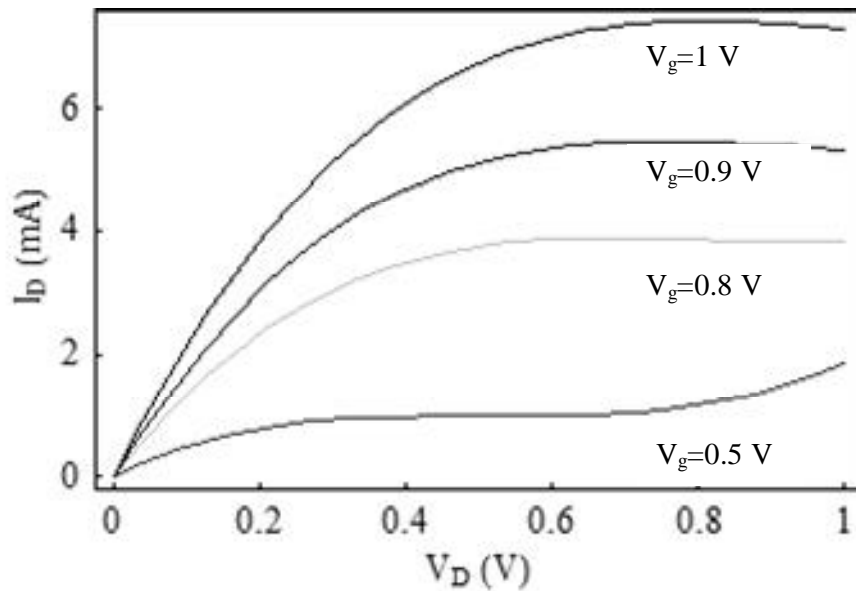


Figure 13 : The  $I_D - V_D$  for various gate voltages

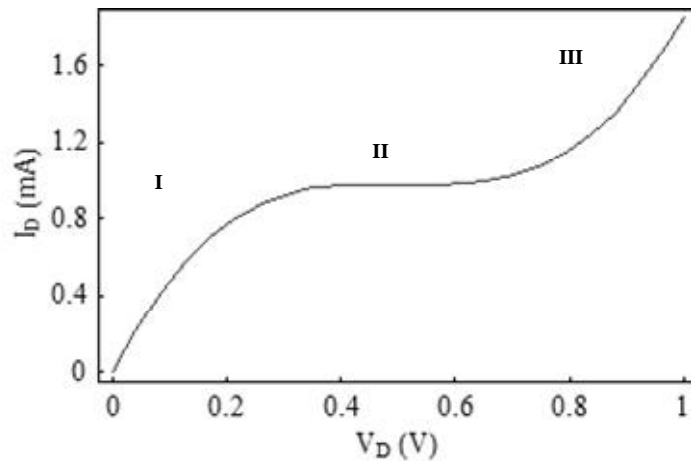
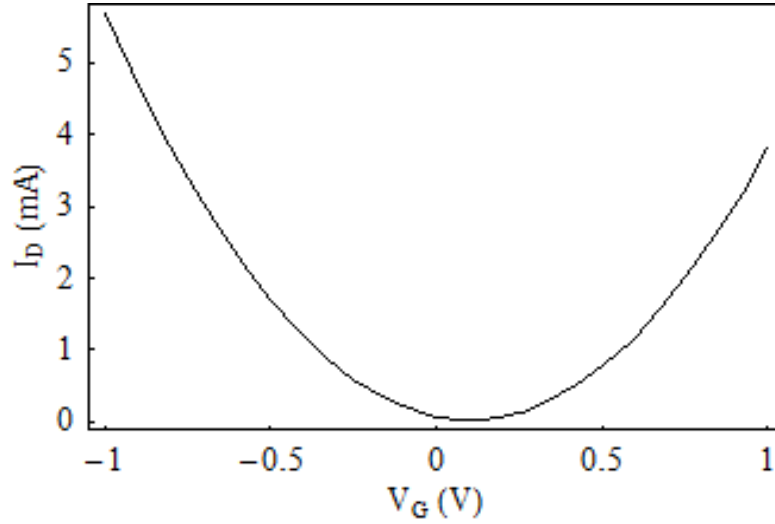


Figure 14 : The three regions of the  $I_D - V_D$  curve at  $V_G=0.5\text{V}$



The  $I_D - V_G$  dependence is displayed in Figure 15 for  $V_D = 0.2 \text{ V}$ . We see that the drain current is not zero even if the gate voltage is zero, a characteristic typical for graphene physics termed as minimum conductivity.



**Figure 15**  $I_D - V_G$  dependence is displayed for  $V_D = 0.2 \text{ V}$ .

The origin of this effect is not well understood, more theories exist to explain this unique phenomenon. The minimum of the  $I_D(V_G)$  curve is the Dirac point for  $V_G = V_{G,Dirac}$ . If  $V_G > V_{G,Dirac}$  we have  $n$ -type conductivity, and if  $V_G < V_{G,Dirac}$  we have  $p$ -type conductivity. The curve has a “V”-letter shape which is retrieved in any graphene FET measurements. The transconductance is a key parameter of any transistor and is defined as  $g_m = \partial I_D / \partial V_g$ . The cutoff frequency of the transistor is directly related to transconductance:

$$f_c = 1 / (2\pi g_m C_{gs}) \quad (6)$$

where  $C_{gs}$  is the gate capacitance.

The transconductance is represented in Figure 16 for the graphene FET with the characteristics displayed above.



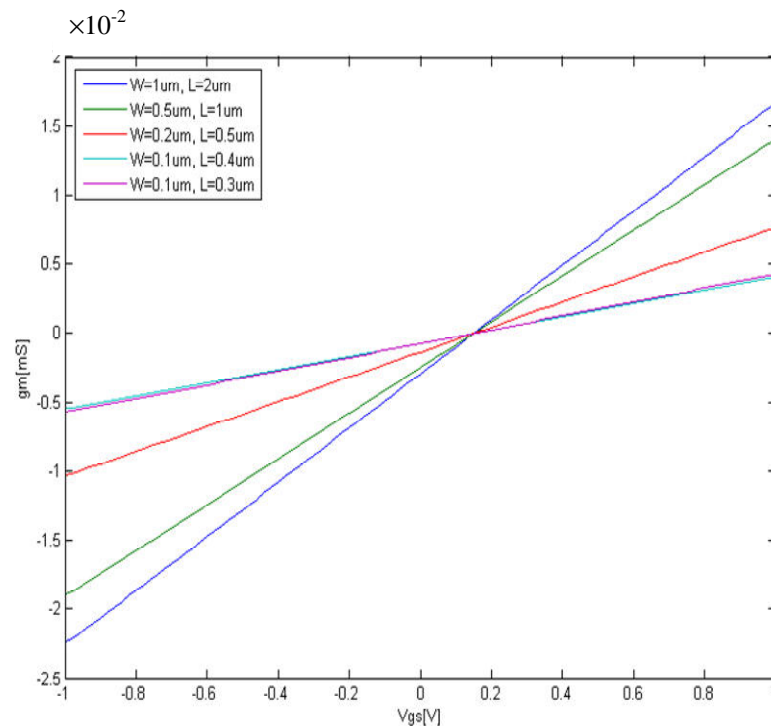


**Figure 16 : The transconductance for graphene FET.**

We can see that the  $g_m$  is small compared to the transconductance of semiconducting FET and this is due to the fact that the graphene monolayer has not a bandgap. The transconductance has positive and negative values due to the ambipolar transport character of graphene.

How we can have then a graphene FET transistor to be used in a LNA :

- There graphene/metal contact is real problem for graphene transistors because its value cannot be decreased under certain limits. Metals with high work function are preferred, because are near of the workfunction of the graphene (-4.5 eV) and these metals produces the low resistance in graphene. In this respect, Ti/Pd/Au displays a contact resistance of  $750 \Omega \mu\text{m}$  which gives a contact resistivity of  $2 \times 10^{-6} \Omega \text{cm}^2$  which is near the state of the art for contact resistance in GaAs technology [14].
- A very high cutoff frequency (see eq. 6) implies a higher  $g_m$  and a low gate capacitance :
  - To increase  $g_m$ , we need an interdigital gate-drain configuration. In [15] with only 3 digit gate-drain array the  $g_m$  is greater with more then one order of magnitude as above i.e.it is  $1 \text{ ms}/\mu\text{m}$  at a gate voltage of 0.6 V or to use as a channel a graphene nanoribbon which has bandgap.
  - We have to decrease the gate capacitance using high electrical permittivity dielectrics like  $\text{HfO}_2$  with a thickness of 2-3 nm. In the WP 3 such gate oxides are specially grown for graphene FETs by Tyndal Institute.
  - Noise in the FETs having a high quality graphene monolayer is much reduced because the number of carriers is reduced in comparison to 3D semiconductor devices. Moreover, in the ballistic case the numbers of collisions between the carriers are much reduced.

We note some particularities of noise properties in graphene FETs [16].

- High quality of graphene (low defects) is crucial for low noise which can reach amplitudes of  $10^{-9}$

- The  $1/f$  noise is not too much increased in the top gate graphene FETs (our case).
- A low dose of electron irradiation (via SEM or EBL) with low energy (20 keV) reduce  $1/f$  noise with one order of magnitude; the consortium has the equipment to this treatment to get low  $1/f$  noise.

A more elaborate model which holds either for ballistic and diffusive regime was developed recently by the authors [17]. The model starts from "Top-of-the-barrier"[18] models generally used for ballistic graphene transistor, but generalize it to any type of transistors.

The method is based on few equations. We consider a top gate transistor where the drain current is given by :

$$I_D = I_n - I_p \quad (7)$$

where the two currents are assigned for electrons and holes, respectively and are described both of them by Landauer formula. The Fermi distributions, the DOS are shifted in energy by the electrostatic potential  $U = U_L + U_P$  which is computed using a lumped element model consisting in capacitor network  $C_G$ , a source  $C_S$  and drain  $C_D$  capacitance. We assume that  $C_S = C_D$ . The source and drain capacitance is a fit parameter. While  $U_L = -e(C_g V_g + C_D V_D)$ , while  $U_P$  is calculated with the help of Poisson relations. The electrostatic potentials are then used to scale the physical parameters of the drain current and finally to calculate the drain current.

Below, we will provide some examples to prove the power of this method which works irrespective of the graphene transport mechanisms.

For example, we are using our own experimental results obtained earlier regarding a graphene FET [19]. The relevant dimensions of the graphene FET are: gate length 200 nm, source-drain distance 2  $\mu\text{m}$  and source-drain width 40  $\mu\text{m}$ . The gate dielectric is a 100 nm thick PMMA layer. The simulated and experimental values of the graphene FET are depicted in Figure 17, also the extracted mean free path is 100 nm (meaning that high quality monolayer graphene), while the maximum mobility was about 8000  $\text{cm}^2/\text{Vs}$ . We see also that at low drain voltages the simulation and experimental results coincide while at high voltages the differences are more important. However, the simulations help us to extract also the physical parameters of graphene and also how to improve the graphene FET.

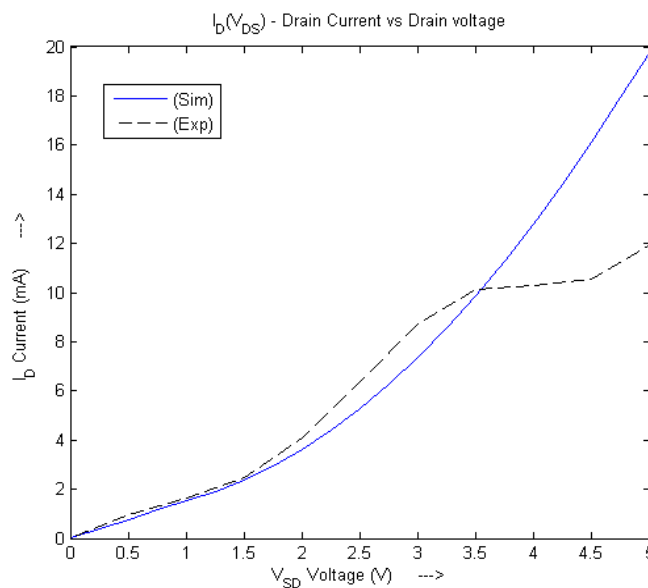


**Figure 17 : The comparison between experimental and simulated values for  $I_D$ - $V_D$ .**

Therefore in Figure 18 we can see how the drain current is improved when the thickness of the dielectric is decreasing.

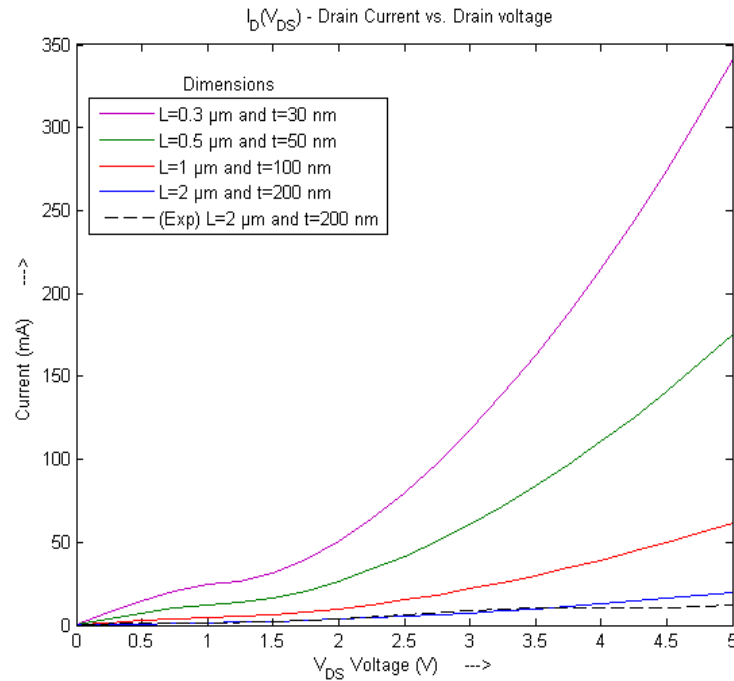


**Figure 18 : The drain current at different dielectric thicknesses.**

So, we can design a graphene FET transistor with a powerful method. When the fabrication of the graphene FET will be completed we will measure the S parameters of the graphene FET and we will design the matching circuits to get a LNA.

### 4 THE DETECTOR

The graphene monolayer rectifier [20],[21] is depicted in Figure 19.

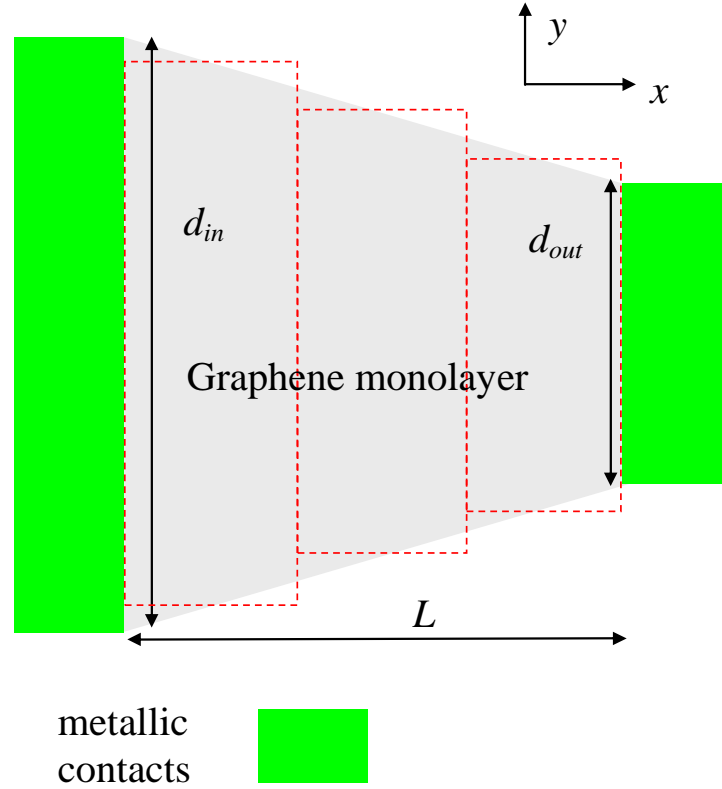


**Figure 19 : The geometric diode based on a graphene monolayer**

In Figure 19, we see that the geometric graphene monolayer diode was modeled as a trapezoidal shape, with the length of the device not exceeding 100-200 nm in order to work in the ballistic regime. We assume that  $d_{in} > d_{out}$ , the rectification being produced for the current flowing parallel to the  $x$  axis. The device is modeled as a succession of  $N$  regions of constant and unequal widths denoted by  $d_j$ ,  $j = in, 1, \dots, out$ .

The wave vector component along  $y$  is discrete and given by  $n\pi/d_j$ , while the wavenumbers along  $x$  are

$$k_{n,j} = \text{sgn}(E - V_j) \sqrt{(E - V_j)^2 / \hbar^2 v_F^2 - (n\pi/d_j)^2},$$

where  $V_j = -jeV/(N+1)$  with  $V$  the bias voltage between the two metallic contacts, and  $v_F \equiv c/300$  is the Fermi velocity. If  $\text{sgn}(E - V_j) > 0$  the carriers are electrons and, on the contrary, if  $\text{sgn}(E - V_j) < 0$  the carriers are holes. The carrier ballistic transport appears in the device only when  $k_{n,j}$  are real. The number of modes is  $N_j = \text{Int}[d_j |E - V_j| / (\pi \hbar v_F)]$ , where  $d_j = d_{in} - (d_{in} - d_{out})j/(N+1)$ .

The simulations regarding the number of modes dependence on the bias voltage are independent on the number of discretization regions  $N$ . In graphene there is a finite number of outgoing modes

irrespective of the voltage polarization, but there is a voltage range around 0 V in which no charge carrier transport occurs, and thus the outgoing mode number and the current are zero. This region of zero current has an extent of  $\pi\hbar v_F / d_{out}$  and is the signature of the rectification behavior of the device. The current-voltage characteristics of the device is found by solving the Dirac equation in each discretized region after imposing the continuity conditions at each interface for the spinorial wavefunction. Further, the current through the triangular-shaped graphene flake is calculated with the Landauer formula. The current-voltage dependence is strongly influenced by the value of  $d_{out}$ . This influence can be seen in Figure 20, where we present simulations for  $E_F = 0.2$  eV and  $d_{in} = 100$  nm,  $d_{out} = 10$  nm (magenta solid line),  $d_{in} = 100$  nm,  $d_{out} = 20$  nm (blue dashed line) and  $d_{in} = 50$  nm,  $d_{out} = 10$  nm (black dotted line).

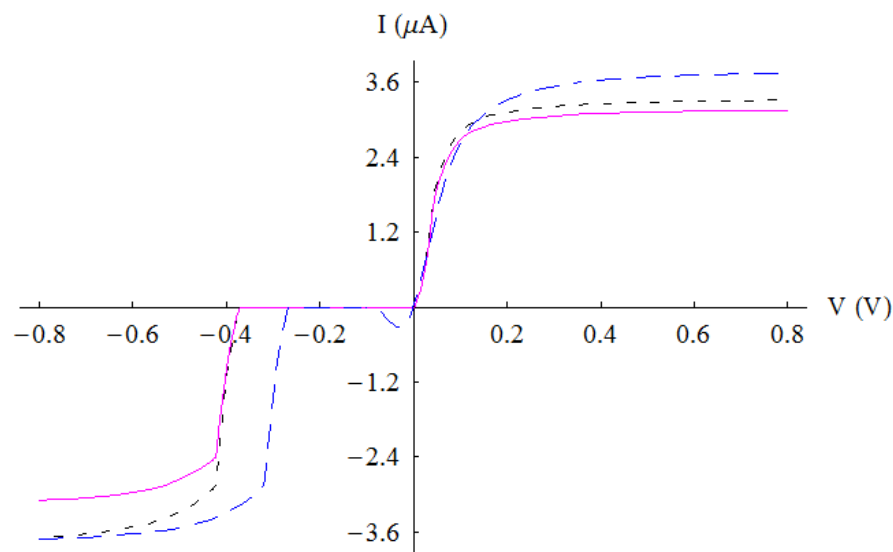


**Figure 20 : The current-voltage characteristics for different  $d_{in}$  and  $d_{out}$  dimensions.**

The fabrication was done mainly to demonstrate that such a new way to build a graphene rectifier is possible. The fabrication details are found in [21] and imply e-beam patterning of the rectifier position on wafer, oxygen plasma cut graphene in the trapezoidal-like shape, followed by another e-beam patterning for contacts and the final liftoff in acetone. The wafer with graphene rectifier is represented in Figure 21 and the graphene rectifiers in Figure 22.

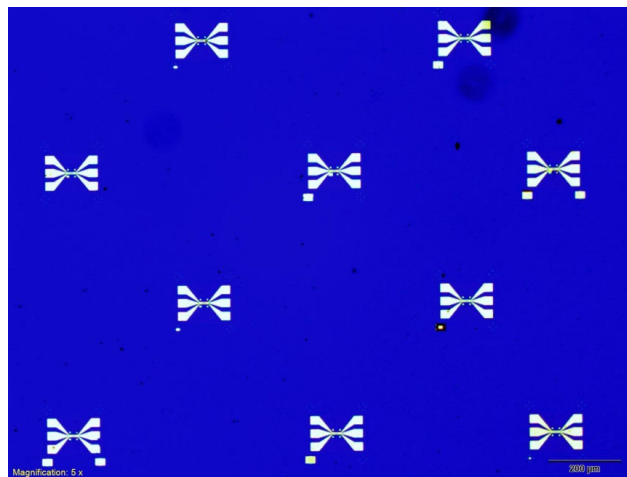
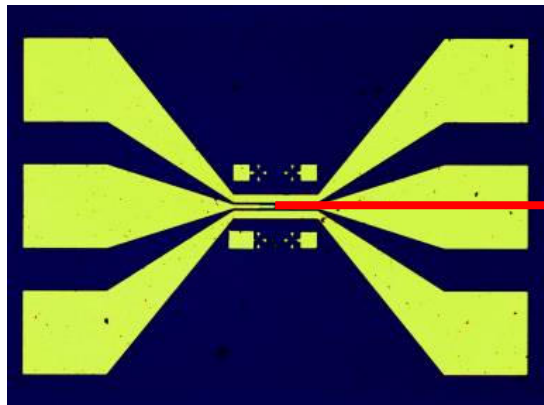
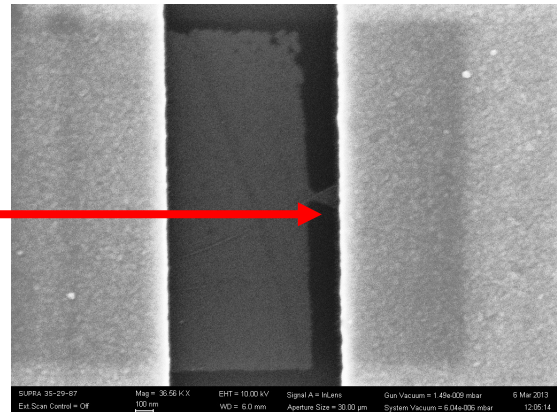


**Figure 21 : The on-wafer view of graphene detector**



(a)



(b)



(c)

**Figure 22 : The graphene rectifier**

In Figure 22 it is represented in (a) the entire structure of the graphene rectifier, (b) the graphene rectifier with metallic contacts (c) the detail of the rectifier –neck diode 28 nm , diode shoulder 100 nm.

The I-V characteristics were obtained using a Keithley 4200 SCS. The graphene wafer with metallic contacts ready to be measured is represented in Figure 23.



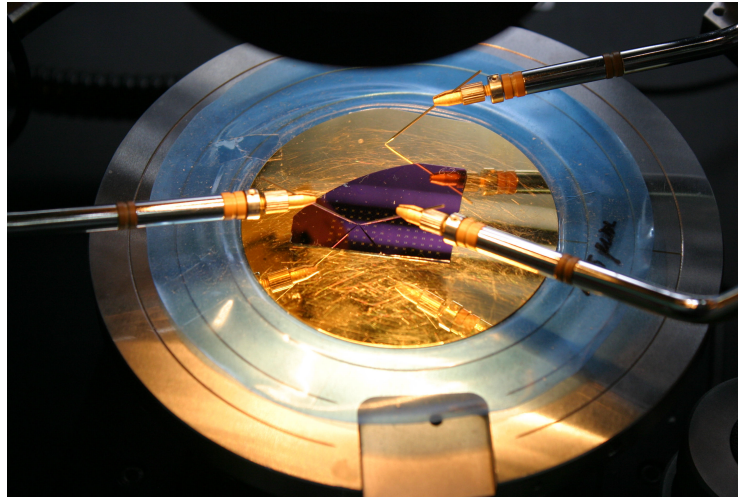


**Figure 23 : Graphene wafer ready to be measured**

In Figure 24 the I-V dependence is displayed.

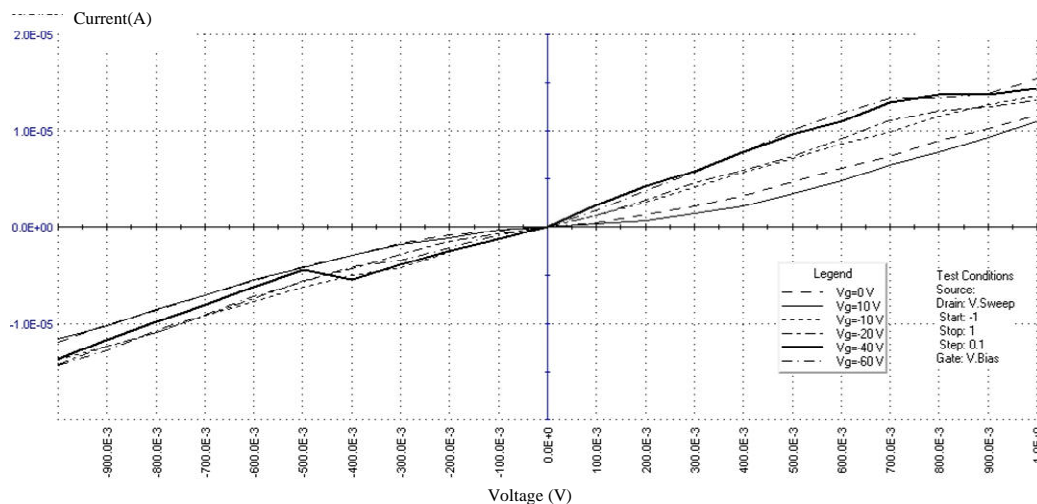


**Figure 24 : The I-V dependence of the rectifier**

We see that at low back gate voltage the curves have a zero current in region of 150 mV so working as a rectifier, while at high back gate voltages (40-60V), this region vanishes and we see the behaviour of a transistor with a back gate and having saturation. Two physical mechanisms are taking place (a) at low back gate voltages we have the ballistic rectification as described by the above modelling while at high back gate voltages the number of so carriers is so high so the graphene constriction is saturated with carriers and the current is constant.

Another rectifier was proposed using the a graphene monolayer shape as below in Figure 25

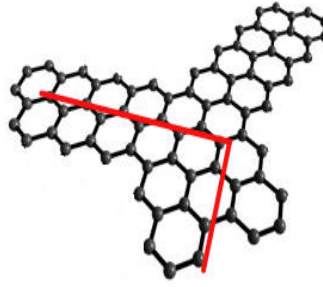


**Figure 25 : The Y rectifier**

The distance between arms is 300 nm while its width is 100 nm and is working also in the ballistic regime. The rectification here is also due the geometry. The interferences between the two arms are at the origin of current rectification. This Y graphene shaped was carved in a CPW between the central conductor and the grounds. We have 2X50 Y –shaped graphene attached to the CPW. The left top and right top edges of each nanoribbon are electrically in contact with the signal and the ground electrode, respectively. To contact the bottom edge of each nanoribbon, without contacting the center of the “Y” shaped graphene junction, a metallic air-bridge is formed between adjacent bottom electrodes. This metallic air-bridge was anchored at the bottom of each “Y” and eventually is electrically connected to the signal electrode that leads to the output port. This rectifier was simulated with the equivalent circuit below in Figure 26.

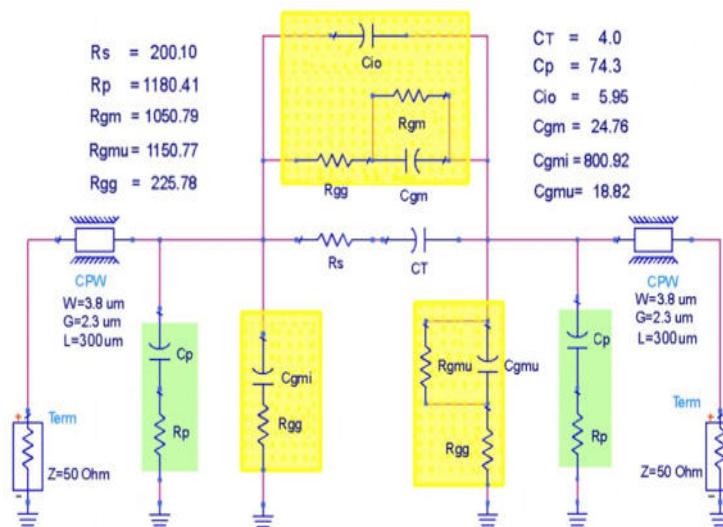


**Figure 26 : The Y rectifier equivalent circuit.**

The rectification can be seen in the current at 20 GHz (Figure 27) where minima and maxima of the current are seen along the central conductor of the CPW



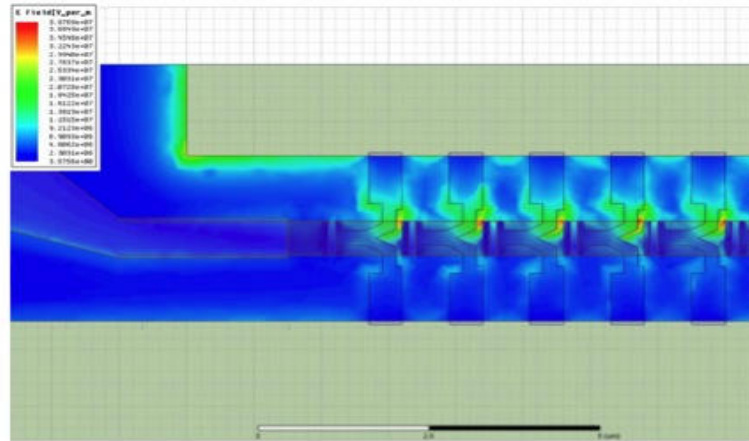


Figure 27 : The rectification current of Y-shaped graphene.

## 5 THE GRAPHENE MIXER

The graphene resistive mixer is based up now on graphene FETs [22]. However, for a high conversion loss (CL) it is necessary that the graphene channel resistance denoted  $R_{ds}$  must have very different values when gate voltage is zero (when  $R_{ds}$  is maximum) and a high gate voltages (when  $R_{ds}$  is minimum) i.e  $R_{ds}(V_g=0)/R_{ds}(V_{g_{max}}) > 15-20$ .

This requirement cannot be fulfilled in graphene monolayer due to the absence of the bandgap. He next was to nanopattern the graphene channel to open small bandgap in the channel. Now  $R_{ds}(V_g=0)/R_{ds}(V_{g_{max}})$  is about 10-12 [23], but the nanopatterning of the graphene is a tedious task and the results are not always reproducible. Of course, a channel with a bilayer graphene will be the bet for a resistive mixer [24] where the ratio  $R_{ds}(V_g=0)/R_{ds}(V_{g_{max}}) > 100$ , but to get such a transistor it is necessary to apply a very high dc field able to destroy the FET anytime.

So, we have decided to abandon the graphene mixers based on FET and to return to a simple solution – a graphene Schottky diode made recently in the consortium [25]. Recently, we have fabricated a Schottky - like diode able to withstand currents at mA level and to operate at millimeter wave frequencies, at which no graphene-based Schottky diode has been reported so far.

To achieve this performance level we have used a graphene monolayer with asymmetric metallic contacts deposited on a high-resistivity Si substrate, with resistivity greater than 8 kΩ, on which 300 nm of SiO<sub>2</sub> were thermally grow.

Schottky contact with graphene with a work function of 4.5 eV is displayed in the Table 2 below. We have used Cr as a Schottky contact

Metal	Work function (eV)
Al	-4.27 eV (the best)
Ti	-4.33 eV

Table 2 : Schottky contact with graphene

The resistive contacts on graphene are displayed in the Table 3 below:

Metal	Work function (eV)
Pd	-5.12 eV
Pt	-5.6 eV
Cr	-4.45 eV (like graphene)

Table 3 : Resistive contacts

We have used Ti as Schottky contact and Cr for resistive contact .The Schottky diode is represented in Figure 28.

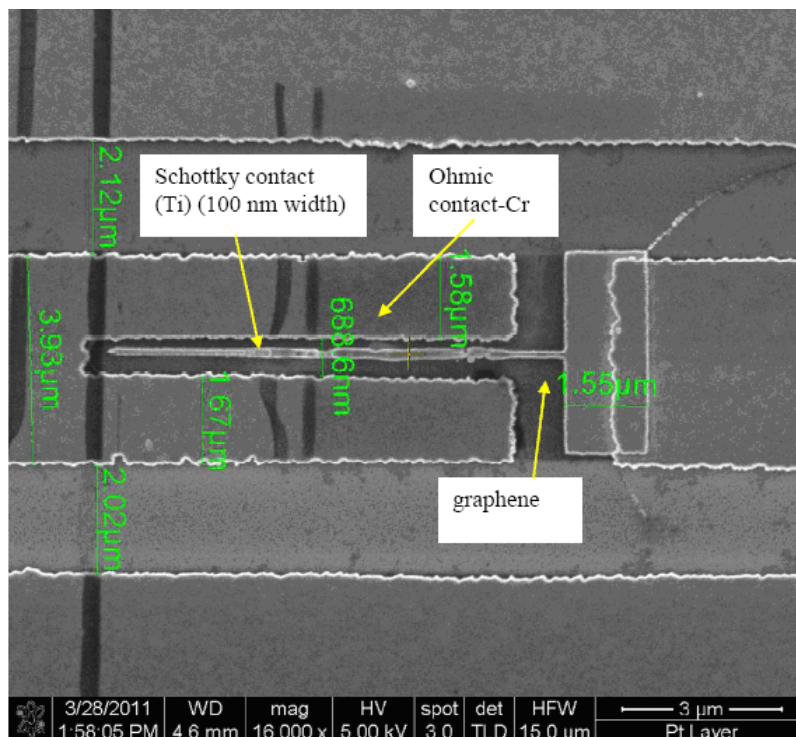


Figure 28 : The Schottky diode on graphene

Extensive measurements in dc and the range 0.04 -60 GHz were performed and an equivalent circuit was extracted. The I-V characteristic is displayed in Figure 29 showing strong nonlinearities either for positive or negative voltages. The device can work also as a rectifier since in the range 0-2V the current is low.

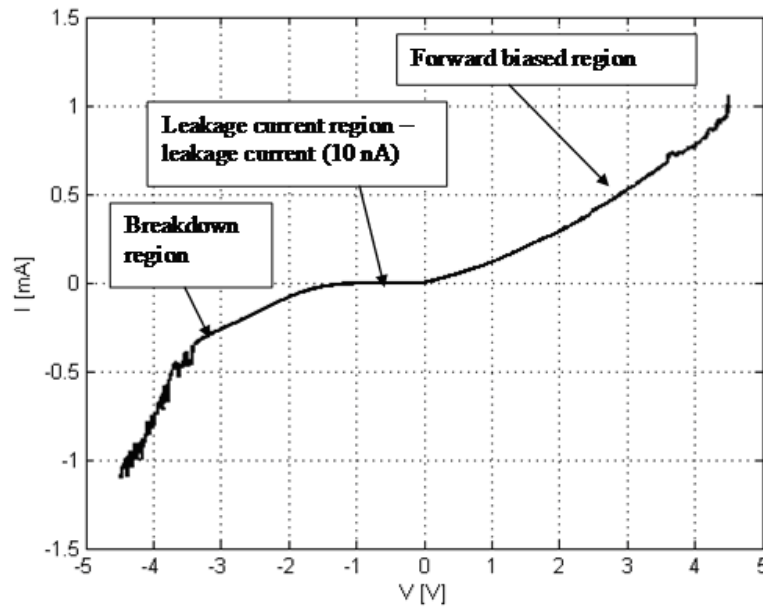


Figure 29 : The I-V dependence of the graphene Schottky diode.

The equivalent circuit is depicted in Figure 30

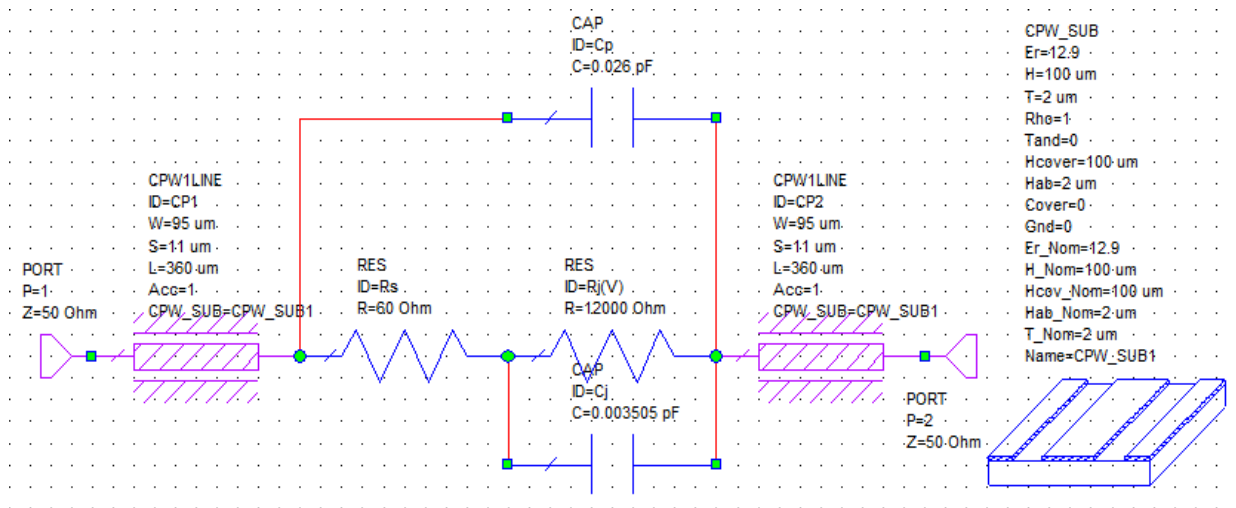


Figure 30 : The equivalent circuit

From many simulations we have extracted the series resistance and capacitance junction values are extracted as it is shown from below Table 4 :

Bias voltage (V)	RS [ $\Omega$ ]	CJ [fF]
0V	60	3.5
1V	60	3.5
2V	60	3.5
3V	60	3.5
4V	60	3.5

**Table 4 : Series resistance and capacitance junction values**

Now, if we consider a quadrature coupler where in two arms are RF signal, LO and the two Schotky diodes the conversion loss is given by [26] :

$$CL(dB) = 3.9 + 1.7/f_c + 9 R_s/Z_0$$

Where  $f_c = 1/2\pi R_s C_j = 75$  GHz

Considering  $f = 10$  GHz and an output impedance of  $100 \Omega$  (which will be transformed latter in  $50 \Omega$ ), we obtain a  $CL = 9.2$  dB

## 6 CONCLUSION

In this deliverable, we presented the design of the different graphene devices which will be made during the project. We have presented a design for graphene antenna, graphene amplifier and a graphene rectifier

### References

- [1] R.S. Shishir and D.K. Ferry, Intrinsic mobility in graphene, J. Phys.: Condens. Matter. **21** 23204 (2009).
- [2] A.S. Mayorov, R.V. Gorbachev, S.V. Morozov, L. Britnell, R. Jail, L.A. Ponomarenko, K.S. Novoselov, K. Watanabe, T. Taniguchi, and A.K. Geim, Micrometer-scale ballistic transport in encapsulated graphene at room temperature, Nano Lett. **11**, 2396 (2011).
- [3] F. Schwierz, Graphene transistors, Nature Nanotech. **5**, 487–496 (2010).
- [4] M. Dragoman and D. Dragoman, Graphene-based quantum electronics, Progr. Quantum Electronics **33**, 165 (2009).

- [5] M.Dragoman, D.Neculoiu, A.Cismaru, A.A. Muller, G. Deligeorgis, G. Konstantinidis, D.Dragoman, and R.Plana, Coplanar waveguide on graphene in the range 40 MHz-110 GHz, Appl. Phys. Lett. 99, 033112 (2011).
- [6] H.S.Skulason, H.V.Nguyen, A. Guermoune, V.Sridharan, M.Siaj, C.Caloz and T.Szkopek, 110 GHz measurement of large –area graphene integrated in low-loss microwave structures, Appl. Phys. Lett. 99, 153504 (2011).
- [7] Hong-Dean Chen, Broadband CPW-fed square slot antennas with a widened tuning stub, IEEE Trans. Antennas and Prop. 51, 1892 (2003).
- [8] G.W. Hanson, Dyadic Green's function and guided surface waves for a surface conductivity model of graphene, J.Appl. Phys. 103, 064302 (2008).
- [9] J.S.Gómez-Díaz, J.Perruisseau-Carrier, P.Sharma and A.Ionescu, Non-contact characterization of graphene surface impedance at micro and millimeter waves, J. Appl.Phys. 111, 114908(2012).
- [10] H.S.Skulason, H.V.Nguyen, A. Guermoune, V.Sridharan, M.Siaj, C.Caloz and T.Szkopek, 110 GHz measurement of large –area graphene integrated in low-loss microwave structures, Appl. Phys. Lett. 99, 153504 (2011).
- [11]S.Rodríguez, R.Yen, L.Liu, D.Jena and H.G. Xiang, Graphene for reconfigurable terahertz optoelectronics, Proc. IEEE 101 , 1705-1716 (2013).
- [12]Liao, Y-C Lin, M. Bao, J. Bai, Y.Liu, Y .Qu, K.L. Wang, Y. Huang and X. Duan, High-speed graphene transistors with self-aligned nanowire gate, Nature , 1-4 (2010).
- [13]K.N.Parrish, and D. Akinwande, An exact solvable model for the graphene transistor in the quantum capacitance limit, Appl. Phys. Lett. 101, 053501 (2012).
- [14] B-C. Huang, M. Zhang, Y. Wang and J. Woo, Contact resistance in top-gated field effect transistors, Appl. Phys. Lett. 032107 (2011).
- [15] S-H Han, K. A. Jenkins, A.V.Garcia , A.D.Franklin, A.A.Bol and W. Haensch, High-frequency graphene voltage amplifier, Nano. Lett 11, 3690-3693 (2010).
- [16].A.A.Balandin, Low-frequency noise 1/f in graphene devices, Nature Nanotechnology 8, 549-559(2013).
- [17] G. Vicenzi, G.Deligeorgis, F. Cocetti, M.Dragoman, L. Pierantoni, D. Mencarelli, R. Plana , Extending ballistic graphene FET lumped element models to diffusive devices, Splid –State Electronics 76 , pp.8-12 (2012).
- [18] G. Liang, N. Neophytou, D. E. Nikonov, and M. S. Lundstrom, “Performance Projections for Ballistic Graphene Nanoribbon Field-Effect Transistors,” IEEE Transactions on Electron Devices, vol. 54, no. 4, pp. 677-682, Apr. 2007.
- [19]G. Deligeorgis, M.Dragoman, D. Neculoiu, D.Dragoman, G.Konstantinidis, A.Cismaru, and R.Plana, Microwave switching of graphene field effect transistor at and from the Dirac point, Appl. Phys. Lett. 96, 103105 (2010).
- [20] D.Dragoman and M.Dragoman, Geometrically induced rectification in two-dimensional ballistic nanodevices, J.Phys. D 46, 055306 (2013).
- [21] . M.Dragoman, A. Dinescu, D.Dragoman,On-Wafer Graphene Diodes for High-frequency Applications, European Solid State Device Research Conference (ESSDERC), Bucharest , September 2013.
- [22] M.A. Andersson, , O.Habibpour, J.Vukusic, and J.Stake, Resistive graphene FET subharmonic mixers: noise and linearity assessment, IEEE MTT 60, 4035-4042 (2012).
- [23] O.Habibpour, J.Vukusic, and J.Stake, A 30 GHz integrated subharmonic mixer based on a multichannel graphene FET, IEEE MTT 61, pp.841-847(2013).
- [24] F. Xia, D.B. Farmer, Y-m .Lin, and P.Avoiris, Graphene field transistor with high on/off current ratio and large transport bandgap at roo temperature, Nano Lett 10 ,pp715-718 (2010).
- [25] M.Dragoman, G. Deligeorgis, A.Muller, A.Cimaru, D.Neculoiu, G. Konstantinidis, D.Dragoman, A.Dinescu and F. Comanescu, Millimeter wave Schottky diode on graphene monolayer via symmetric metal contacts, J. Appl. Phys. 112, 084302 (2012).
- [26]Agilent white paper A 5–6 GHz Schottky Diode Single Balanced Mixer



## **D2.5 : Report on the design of graphene devices**

30/30